

Article

The Structural Performance of Reinforced Concrete Members with Monolithic Non-Structural Walls under Static and Dynamic Loads

Walid Ahmad Safi ^{1,*}, Yo Hibino ², Koichi Kusunoki ³, Tomohisa Mukai ⁴ , Yasushi Sanada ⁵, Izumi Nakamura ⁶ and Satoru Fukai ⁷

¹ Graduate School of Engineering, Hiroshima University, Higashi-Hiroshima 739-8527, Japan

² Graduate School of Environmental Studies, Nagoya University, Nagoya 464-8603, Japan; hibino@nuac.nagoya-u.ac.jp

³ Earthquake Research Institute, The University of Tokyo, Bunkyo-ku 113-0032, Japan; kusunoki@eri.u-tokyo.ac.jp

⁴ Building Research Institute, Tsukuba 305-0802, Japan; t_mukai@kenken.go.jp

⁵ Graduate School of Engineering, Osaka University, Suita 565-0871, Japan; sanada@arch.eng.osaka-u.ac.jp

⁶ National Research Institute for Earth Science and Disaster, Tsukuba 305-0006, Japan; izumi@bosai.go.jp

⁷ Structural Engineering Division, Nikken Sekkei Ltd, Chiyoda-ku 102-0072, Japan; fukai@nikken.jp

* Correspondence: d174422@hiroshima-u.ac.jp; Tel.: +81-80-5962-4406

Received: 19 March 2020; Accepted: 20 April 2020; Published: 6 May 2020



Abstract: The required base shear and drift limit for post-disaster management buildings have increased in the Japanese Building Code following major seismic events. One method to satisfy these requirements for reinforced concrete frame buildings is to cast exterior non-structural concrete wall elements to be monolithic with frame elements, but without anchoring the longitudinal wall reinforcing. This provides additional stiffness and strength while limiting significant damage in the non-structural wall. In this study, the structural performances of such elements were evaluated using static and dynamic experimental tests. The result indicates that non-structural walls that were neither isolated by seismic slits nor anchored to the adjacent walls with longitudinal reinforcements experienced less damage and higher deformability compared with walls having seismic slits. The confinement reinforcing impact was not observed on the strength and drift capacity of the beam member, owing to the large number of transverse reinforcements. However, the confinements limited the damage and nearly prevented concrete crushing. The maximum horizontal load of the specimen could be predicted using cross-sectional analysis, and the authors propose a simple equation to predict it with sufficient accuracy.

Keywords: non-structural wall; dynamic response; static response; flexural strength; drift capacity; seismic design

1. Introduction

The wall members which are supposed to be non-load bearing components in a reinforced concrete building, are referred to as non-structural elements; however, their usage and design philosophy are changed following each significant earthquake. The Japanese building standards which were amended in 1981, allowed for the premature failure of non-structural walls, in situations where it did not adversely affect the structural member. Damage observations of the reinforced concrete buildings after Great Hanshin earthquake in 1995 showed that the structural damage was minor compared to non-structural walls, which were reportedly significantly damaged [1]. In addition, the non-structural walls were severely damaged in the aftermath of the Great Tohoku earthquake 2011. That outcome

tends to adversely influence the structural performance of the frame and decrease the possibility of continuous usage of these buildings in post-disaster management scenarios [2].

Recently, containing damage to the non-structural walls by avoiding stress transmission using seismic slits has been encouraged. The presence of a seismic slit between a non-structural wall and a primary frame restrains the stress transmission from the structural frame to non-structural walls to limit the damage [3]. However, in practice, the seismic slit often appears as a result of monolithic casting of the non-structural wall with a frame which cannot completely isolate the non-structural wall. Besides complicating the design principles, the seismic slit allows the stress transmission to affect the capability of the main members and the rigidity of the buildings, considering the significance of the strength and rigidity of a building.

The shape of a non-structural wall is determined by the shape of its opening, which may cause vulnerability during significant earthquakes. Damage to the non-structural walls may significantly reduce functionality and continuous usage of the post-disaster buildings after earthquakes, owing to a large number of cracks and plastic hinges at the end of the wall and the members.

In past significant seismic events in Japan, reinforced concrete buildings, which were expected to be used as disaster management facilities following earthquakes, suffered severe damage and could not be used for post-disaster functions as intended [4]. A design guideline for disaster base facilities provided by the National Institute for Land and Infrastructure Management (NILIM) recommends the utilization of non-structural wall components made of reinforced concrete, such as wing walls and spandrel walls, to increase the drift capacity of members and provide capability for continued use of buildings by casting them to be monolithic with structural members [5]. Under the current design practices in Japan, reinforced concrete non-structural walls are often isolated from the moment-resisting frames by seismic slits installed between the wall segments and the primary frame. The presence of a seismic slit might reduce the strength capacity of the beam, and induces the formation of plastic hinges. Removal or reduction of the seismic slit increases the strength of a member and helps it meet the NILIM-required criteria for disaster management facilities. The NILIM guidelines mandate that disaster management buildings shall satisfy requirements for disaster base facilities, which are as follows:

1. The base shear coefficient shall be 0.55 in a case in which the non-structural walls are available. The aim of that is to ensure the serviceability of the building during and after earthquakes. Besides this, a limit of inter-story drift shall be less than 0.33%.
2. The base shear coefficient shall be 0.3 in a case in which the non-structural walls are not available due to damage by an earthquake, the aim of which is to ensure the safety of the building after earthquakes.

The above two requirements were made based on the concept that the building must serve as a disaster base facility during and after an earthquake.

The results from an experimental test with reinforced concrete moment resisting frames with non-structural wing walls casted to be monolithic with frame elements showed higher initial stiffness and lateral strength in the member with the monolithic non-structural wall [3]. However, significant strength degradation was observed after the lateral strength peak was reached. This degradation was assumed to be caused by the damage in non-structural walls, where the longitudinal reinforcement was tied into the structural system. To minimize damage to the wing walls due to wall reinforcement, it was suggested that the reinforcement within these non-structural walls be terminated before at the end of the walls rather than being anchored into other elements [6]. In the proposed modification, the influence of confinement transverse reinforcement (the volume of which can be determined based on Architecture Institute of Japan (AIJ) standards [7], and American Concrete Institute (ACI) code [8]) on the drift capacity of non-structural wall members was investigated.

The objective of this study was to investigate the seismic performances of beams having non-structural spandrel walls without seismic slits. In addition, we intended to ascertain the impacts

of AIJ and ACI-based designed confinement reinforcements, which are placed in the critical strips of spandrel walls. Moreover, this study aimed to develop a new detailing method for members which are required to exhibit higher seismic performance, and to verify the proposed method using experimental tests. Tests were performed with reinforced concrete beams with non-structural walls attached using the proposed detailing method. Furthermore, the method was assessed for hanging walls through an artificial earthquake in a real three-story building to verify its effectiveness.

2. Detail of Proposed Method

A new detailing method for the connection of a non-structural spandrel wall with either a column or another wing wall is proposed herein. The beam has a non-structural hanging or standing wall casted to be monolithic with the frame elements. These walls are also casted to be monolithic with other walls or columns at their ends with reduced seismic slits, as shown in Figure 1a.

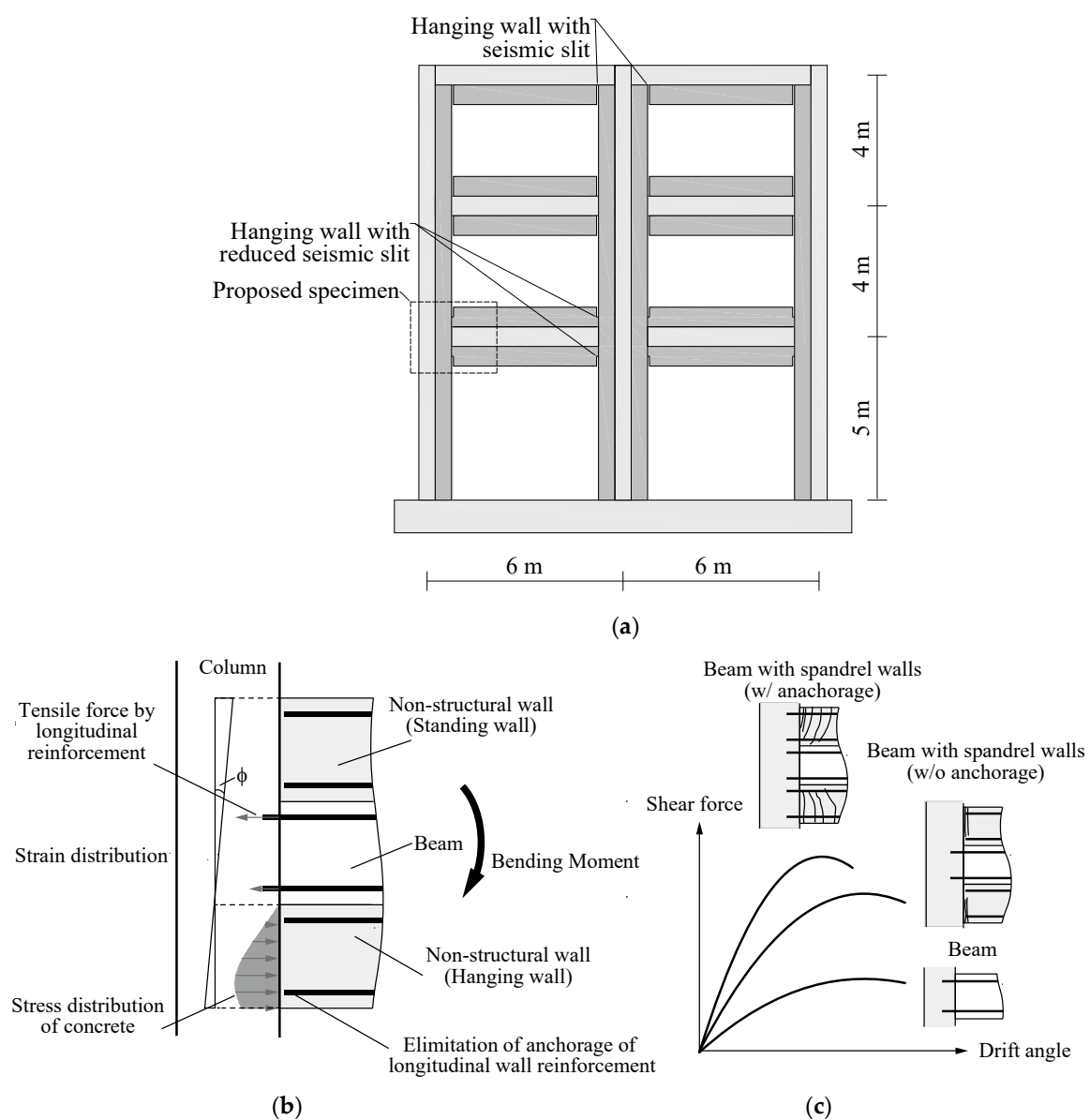


Figure 1. Proposed new detailing of reinforced concrete member with non-structural walls: (a) specimen position in the frame; (b) working mechanism; (c) expected performance.

As part of this proposed method, longitudinal reinforcement within the spandrel wall should not be anchored into the adjacent member, as shown in Figure 1b; hence, this type of detailing is referred to as non-anchored detailing. When the anchorage of a longitudinal wall reinforcement is eliminated, cracks then generally only occur at the wall's ends, which prevents significant spread of cracks along the wall's length. Furthermore, the wall would only contribute in compression, which increases initial stiffness and lateral strength moderately compared to using seismic slits. In summary, a beam member with spandrel wall whose longitudinal wall reinforcement is not anchored has greater deformability compared with an anchored one, while a beam without non-structural spandrels would have a lower capability compared with anchored and non-anchored detailing beam members, as shown in Figure 1c. The anchorage of longitudinal wall reinforcements results in possible buckling of the reinforcements and a different bonding mechanism with the concrete compared to non-anchored detailing, which relatively affects the drift and strength capacity.

3. Static Evaluation of the Proposed Detailing Method

3.1. Test Specimens

Two full-scale specimens named BSH and BS were designed and tested under cyclic loading. The first letter B in BSH and BS stands for beam, S for spandrel wall and H for having confinements. The specimens were meant to verify the performance of the proposed method regarding an isolated, non-structural spandrel wall attached to a beam. The structural properties of the specimen were determined based on required demand forces for disaster management facilities. The specimen simulated a beam in the structural frame, which had spandrel walls as shown in Figure 2.

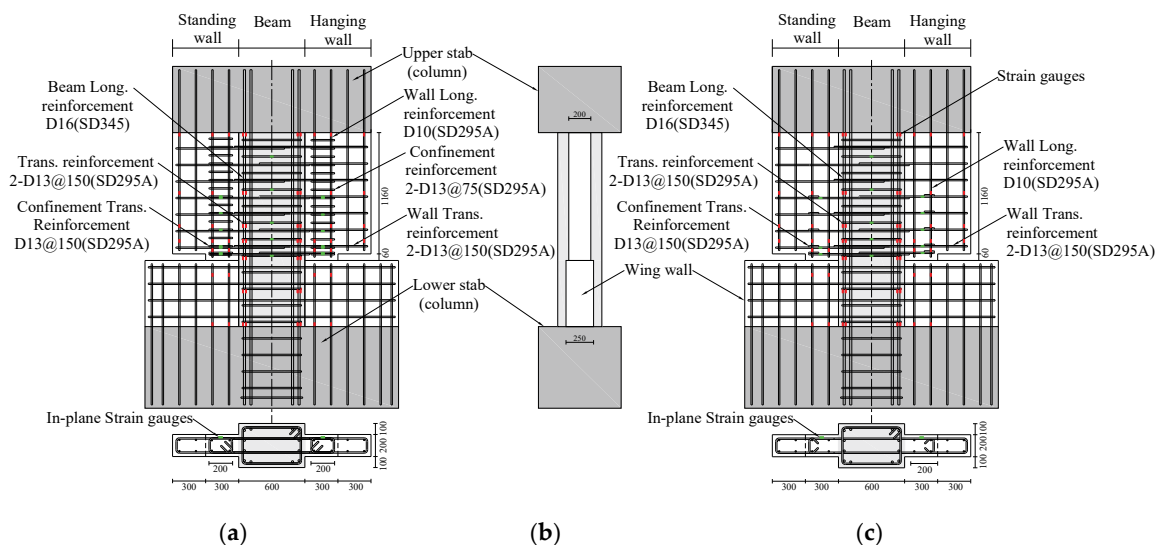


Figure 2. Geometry of specimen; (a) in-plane view of BSH; (b) out of plane view of BSH and BS; (c) in-plane view of BS. The first letter B in BSH and BS stands for beam, S for spandrel wall and H for having confinements.

The reinforcement details of the specimen are shown Table 1; concrete and steel properties of the specimens which were obtained from concrete cylinder compression and bar tensile pull tests are shown in Figure 3 and Tables 2 and 3.

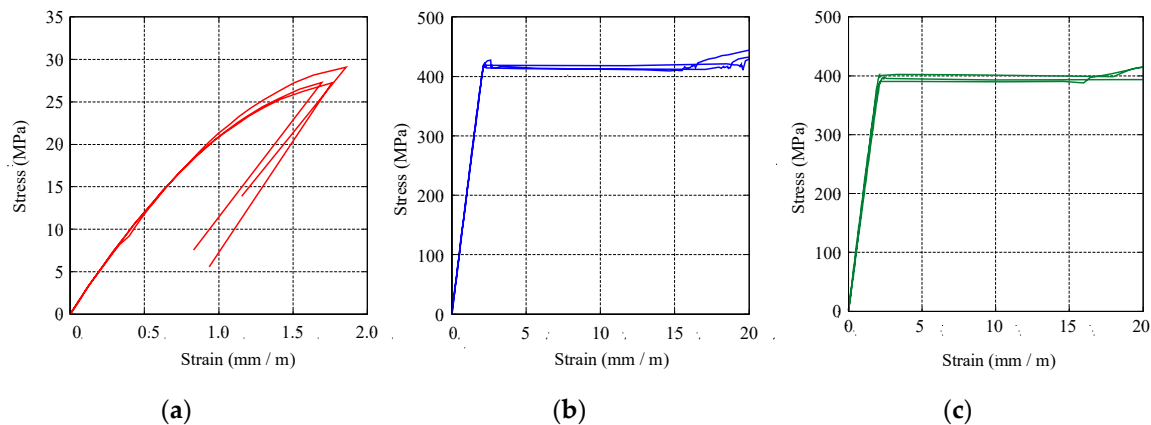


Figure 3. Stress–strain relation: (a) concrete of BSH and BS; (b) steel bar D13; (c) steel bar D19.

Table 1. Details of specimens.

Name	BSH	BS
Type of member ($B \times D$)	Beam (400 mm \times 600 mm)	
Long. reinforcement	12-D19 ($\rho_g = 1.56\%$)	
Trans. reinforcement	D13@150 ($\rho_t = 0.42\%$)	
Wall type (Thickness)	Spandrel Walls (200 mm)	
Length of walls (mm)	600 (300 at the wall boundary)	
Long. wall reinforcement	2-D13@150	
Trans. wall reinforcement	2-D13@150 (0.84%)	
Design of confinement reinforcement	ACI	AIJ
Confinement reinforcement (X)	2-D13@75 (2.54%)	(0.85 %)
Confinement reinforcement (Y)	2-D13@75 (1.13%)	D13@150 (0.15%)
Initial target load (kN)	88 (1st) and 162 (2nd)	
Target drift angle R (rad)	$\pm 1/400, \pm 1/300, \pm 1/200, \pm 1/150, \pm 1/75, \pm 1/50, \pm 1/37.5, \pm 1/25$	

Table 2. Concrete properties.

	BSH	BS
Compressive strength (MPa)	27.9	30.0
Young's modulus (MPa)	23.9×10^3	26.9×10^3

Table 3. Steel properties.

Number	D13	D19
Type	SD295A	SD345
Yield stress (MPa)	423	397
Tensile stress (MPa)	600	579
Young's modulus (MPa)	202×10^3	194×10^3

The specimens BSH and BS were fabricated as beams with non-structural spandrel walls; thus, the spandrel wall was attached to the wing wall without a seismic slit in the critical area. As shown in Figure 2, the specimen BSH and BS consisted of beams, spandrel walls and wing walls. The wing walls were placed horizontally below the wall boundaries; hence, the footing beam effectively serves as a column. The wall length was 600 mm, which corresponded to the depth of the beam; however, at the wall boundary cross-section, the length was reduced to 300 mm because the moment capacity tended to be attributed to the wall length. The confinement reinforcement at the wall boundary was determined based on the AIJ and ACI codes. The amount of the confinement reinforcement specified

by the ACI code was larger than that of the AIJ code. The confinement reinforcement ratio in each direction included the amount of the wall reinforcement.

The main parameters of the specimens are the respective existence and non-existence of the confinement reinforcement placed in the wall's critical strip, as shown in Figure 2. The numbers of longitudinal and transverse reinforcements of the members were determined based on required moment capacity and shear force assumed in the design under consideration. The confinement reinforcement at the wall boundary was designed according to the boundary element specified in the ACI code [8], and the design standard for reinforced concrete buildings in Japan [7]. As previously mentioned, none of the longitudinal wall reinforcing bars were anchored.

Figure 4 shows the diagram of the experimental setup which was carried out in the experimental facilities of Hiroshima University. The vertical jack was used to avoid applying the axial load on the specimen, while the horizontal jack was used to apply horizontal load to the center of loading beam. The lower stab of the specimen was fixed-end, and asymmetric loading was performed in a cantilever form on the center of upper stab. The upper stab was fixed to the loading beam of machine and the lower stab was fixed to the floor. Each stab was hold by installing of eight numbers of threaded rods. A 200 kN force was applied for tightening of each rod to fix the upper stab and a 300 kN force was applied for tightening of each rod to fix the lower stab. These forces were used to avoid overturning and torsional effects on the specimen.

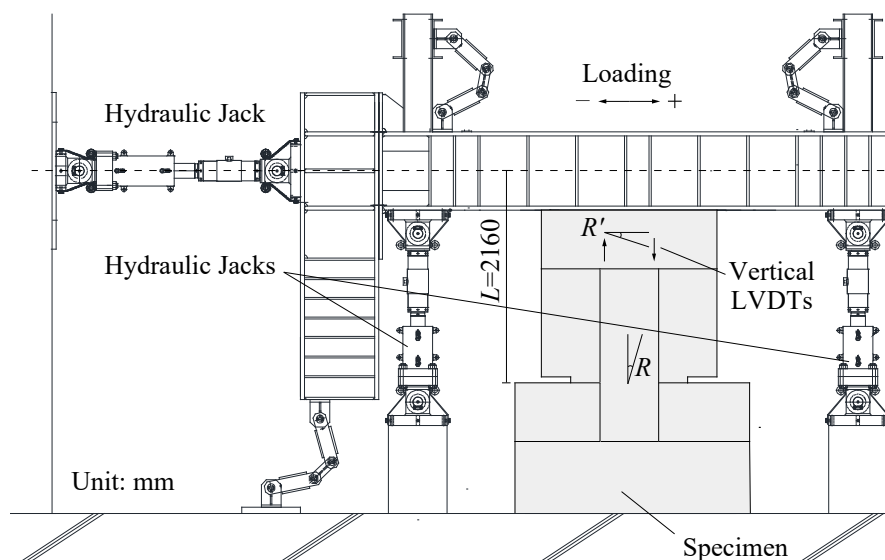


Figure 4. Experimental setup.

The cyclic loading test was conducted by controlling the target horizontal load and drift angle. The loading started from the initial target load, as shown in Table 1. The loads were designed based on the allowable stress design limit. After the initial loading, the specimen was pushed until it reached the target drift angle R , which was measured by linear variable differential transformers (LVDTs). As shown in Figure 5, the X1 and X2 LVDTs were used to measure the total horizontal displacement of the specimen; Y1 and Y2 to control vertical displacement; the R and L series of LVDTs were used to measure right and left spandrel movements; B and H series were used to measure beam diagonal and horizontal movements respectively.

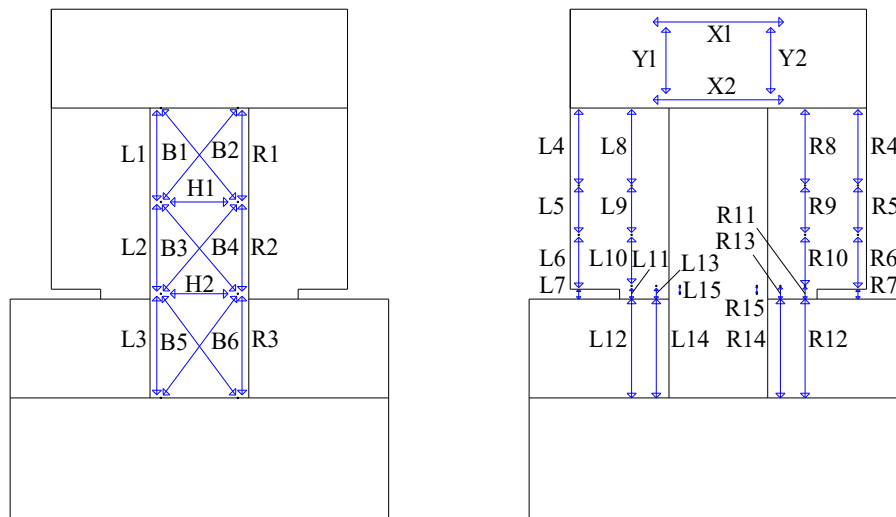


Figure 5. Locations of the linear variable differential transformers (LVDTs) on the surfaces of specimens BSH and BS.

3.2. Test Results

3.2.1. Relationship between Horizontal Load and Drift Angle

The relationships between horizontal load and lateral displacement are shown in Figure 6. The square and circle symbols represent the yielding of the longitudinal reinforcement and peak horizontal load observed, respectively. The dashed lines represent the analytical predictions for the specimen, which were obtained from the moment–curvature relationship using cross-sectional analysis software Response-2000 [9]. Response-2000 allows analysis of beams and columns subjected to arbitrary combinations of axial load, moment and shear. It also includes a method to integrate the sectional behavior for simple prismatic beam-segments. The assumptions implicit in the program are that plane sections remain plane, and that there is no transverse clamping stress across the depth of the beam.

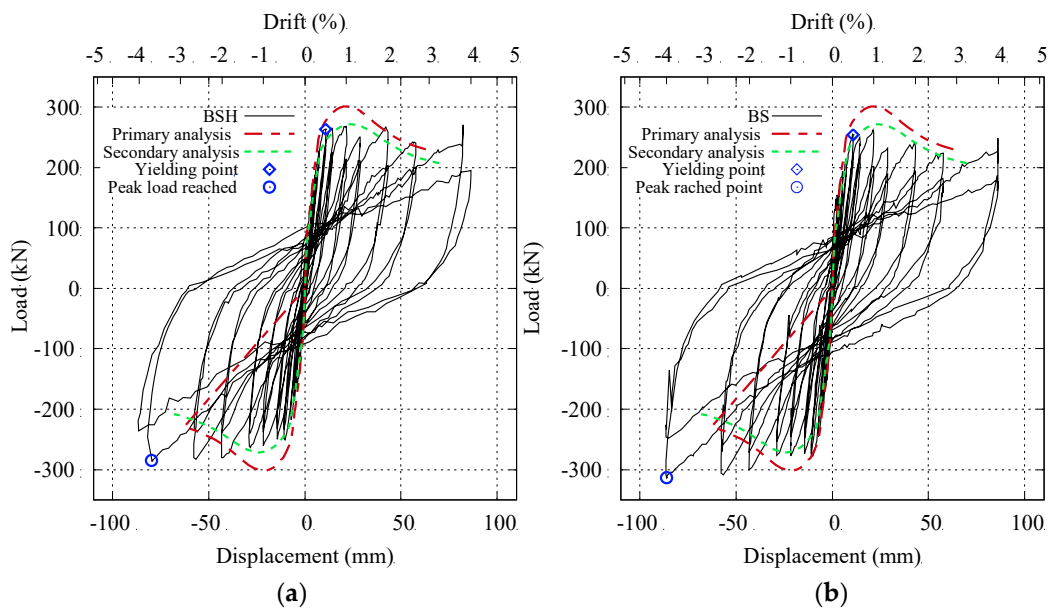


Figure 6. Relationship between horizontal load and lateral displacement: (a) BSH; (b) BS.

Both specimens’ sections were modeled in Response-2000 based on their detailed material properties obtained from the experimental testing results. The concrete stress–strain curve was assumed based on

the Popovics model [10], and steel's stress–strain relation was developed according to the modified input data, as shown in Figure 7.

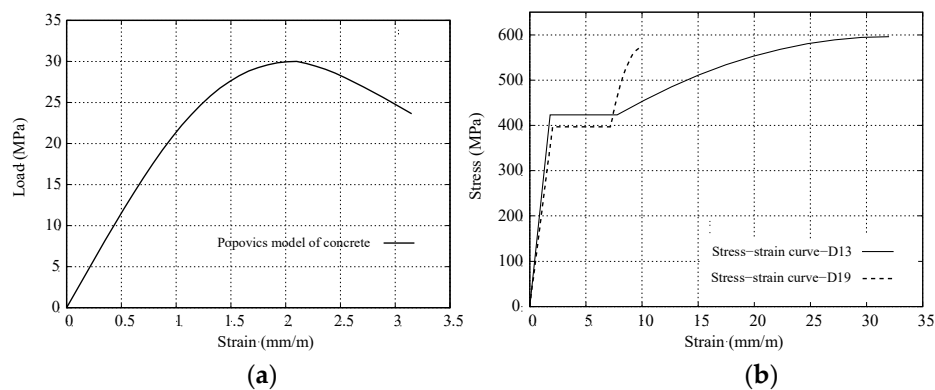


Figure 7. Analytical stress–strain model: (a) concrete; (b) reinforcement.

The primary analytical prediction is shown in Figure 6. The shear span length of the beam was assumed to be 2160 mm and was refined after understanding the exact shear span length that was observed during the test.

The specimen BSH and BS showed similar trends. Firstly, bending cracks occurred during initial loading cycle. Secondly, the longitudinal reinforcement of beam in both specimens yielded at $1/200$ rad and minor stiffness degradation was seen. Thirdly, compression failure in the concrete cover of the non-structural wall was observed at $1/150$ rad for both specimens. Afterwards, slip behavior was seen for both specimens following yielding of the longitudinal reinforcement. Finally, the horizontal load increased until reaching the peaks of 285 and 313 kN for specimens BSH and BS, respectively, at $1/25$ rad drift angle. The maximum horizontal load nearly agreed with the predicted shear strength using cross-sectional analysis. Moreover, high performances were observed from both specimens regardless of the amount of the confinement reinforcement for the range of drift demands considered. Thus, it was confirmed that non-anchorage of the longitudinal spandrel wall reinforcement and reduction of the seismic slit increased flexural moment capacity and deformability to the structural member.

3.2.2. Cracking Behavior

Crack patterns in both specimens were drawn at a $1/100$ rad drift angle, as shown in Figure 8. The painted area represents the spalling area of the concrete. The bending cracks appeared in the spandrels at a drift angle of $1/200$ rad and extended diagonally into the structural system as the drift angle increased. The spandrel walls of the beam showed dominant flexural behavior compared with the beam itself, owing to a larger cross-section at the middle of the spandrel wall than at its ends. The spalling area in the concrete was influenced by the amount of confinement reinforcement.

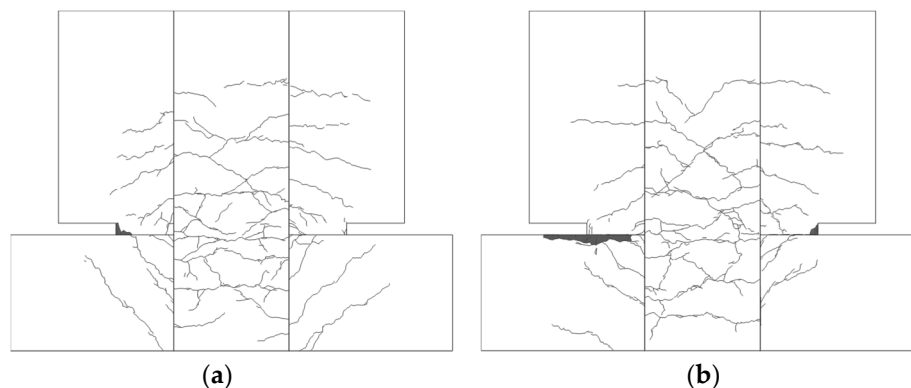


Figure 8. Crack patterns at $1/100$ drift: (a) BSH; (b) BS.

Figure 9 shows the relationship between residual crack width and drift angle. The width was measured on the structural member and the wall. The crack width was observed to increase with increasing drift angle; however, a dominant wider crack was observed at the wing–wall interface in both specimens because the longitudinal wall reinforcement was not tied to the footing beam.

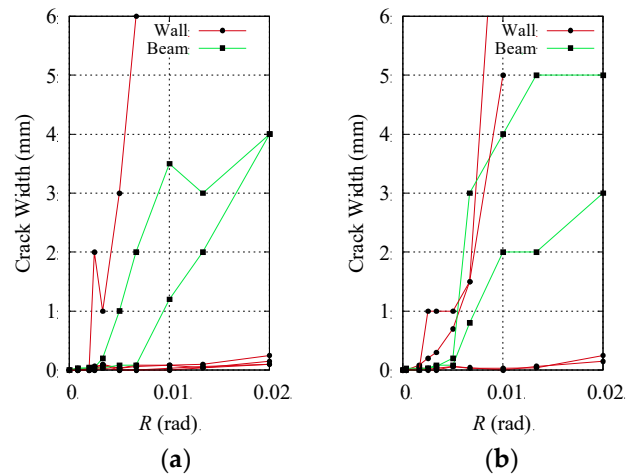


Figure 9. History of residual crack width: (a) BSH; (b) BS.

The cracks with similar colors in Figure 9 declare the dominant observed cracks of the elements of the specimens in the similar loading scenario. The dominant cracks between the wall boundary and the footing beam occurred at a drift angle of 1/50 rad, as shown in Figure 10.

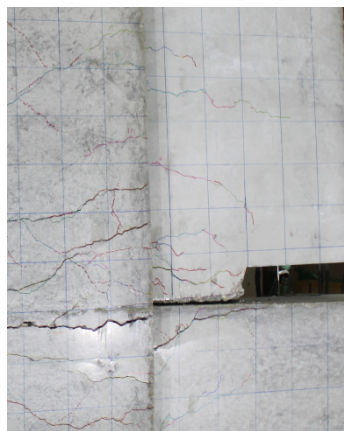


Figure 10. Dominant large crack.

3.2.3. Stress Distributions

The stress distribution of the longitudinal reinforcement is shown in Figure 11. The stresses were determined by the strains, which were recorded using strain gauges installed at the longitudinal reinforcements, as shown in Figure 2, assuming bilinear hysteretic stress–strain behavior for the steel reinforcements. The longitudinal reinforcement of the beam yielded in tension, while tension stresses in the longitudinal wall reinforcement for both specimens were negligible owing to the non-anchorage detailing. However, the longitudinal wall reinforcements experienced noticeable compressive stresses. The neutral axis depth appeared to be in the boundary between the walls and a structural member.

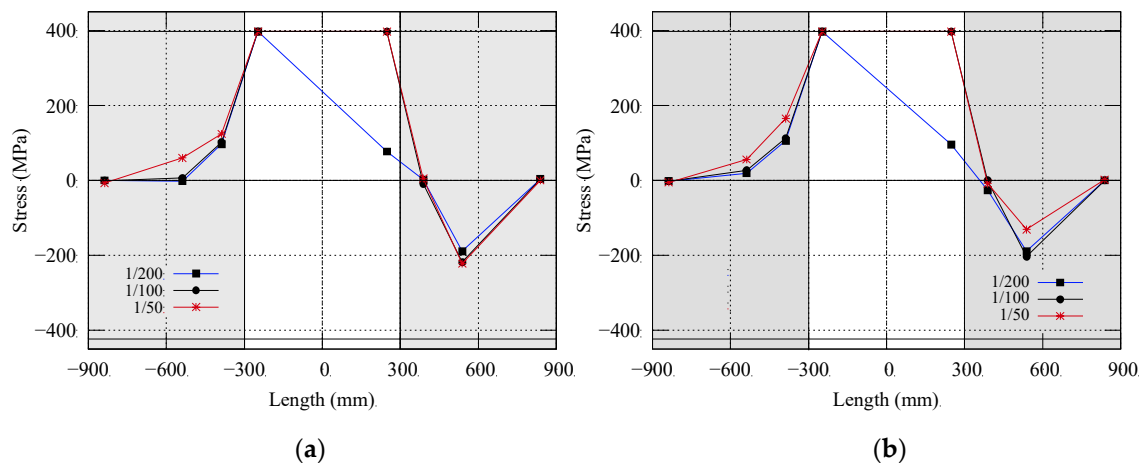


Figure 11. Stress distributions of longitudinal reinforcements: (a) BSH; (b) BS.

Figure 12 shows the stress distributions of confinement reinforcements. The vertical axis represents the height of the strain gauges, and the horizontal axis represents the stress. The strain gauges were installed at the reinforcements both in-plane and out of the loading plane, as shown in Figure 2. For specimen BS, the stress at the wall boundary was compressive owing to the axial force at the concrete, as can be seen in the stress at the longitudinal wall reinforcement in Figure 11a,b. Thus, installation of confinement reinforcement at the wall boundary can be effective in damage restriction; however, as previously shown in Figure 6, the impact of confinement reinforcement on the strength of the element was not obvious in this study.

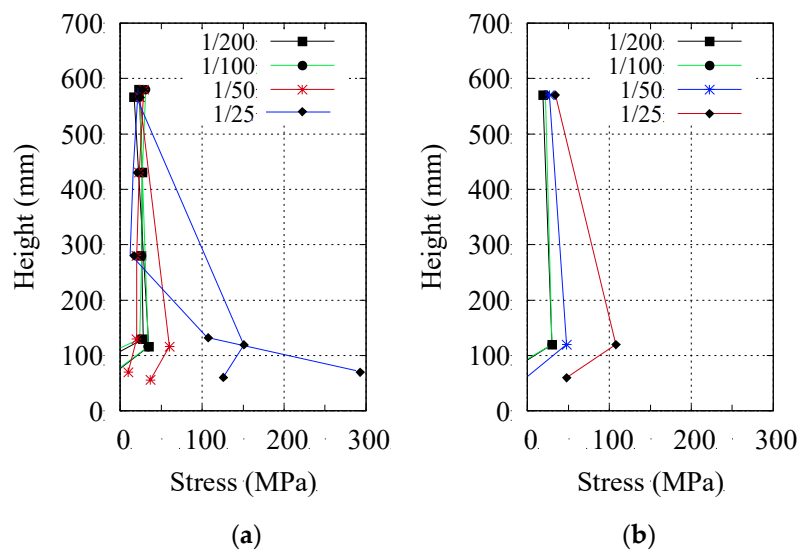


Figure 12. Stress distributions of confinement reinforcements: (a) BSH; (b) BS.

3.2.4. Prediction of Shear Span Length

Since the wall boundary of the beam specimen was connected to the wing walls, the critical cross-section was not clear. The critical cross-sections of the beam and of the non-structural walls extended to the inside of the wing wall, causing cracks on the wing walls. When calculating the bending moment from shear force or vice versa, shear span length should be considered. The section where dominant horizontal cracks were observed can be considered the critical section. However, as can be seen in Figure 8, cracks were well distributed around the beam-wing-wall interface, and thus the boundary cannot be easily defined. Another way to estimate the critical cross-section is by considering the drift angle and displacement. The length L' from the loading point to the critical section, which represents

shear span length, was derived by $L' = R'/\delta$ (where R' is drift angle measured by LVDTs, as shown in Figure 4; δ is displacement at the top of the specimen).

Figure 13 shows the relationship between estimated shear span length and drift angle in each loading direction. The dashed line represents the average of all data, while the red solid horizontal line at 2160 mm was the length L from the loading point to the wing-wall boundary. The shear span length at smaller drift angle was varied, but it became closer to 2160 mm at 1/50 rad, where the longitudinal reinforcement yielded. The average estimated length was 2375 mm at 1/200 rad, which indicated that the shear span length was 200 mm deeper from the surface of the wing wall due to cracks on the wing walls. The secondary analytical predictions for both specimens, as shown in Figure 6, were obtained from the sectional analysis considering the average value at each respective drift of Figure 13, which was closer to the experimental result compared to the primary analytical prediction obtained using a shear length of 2160 mm.

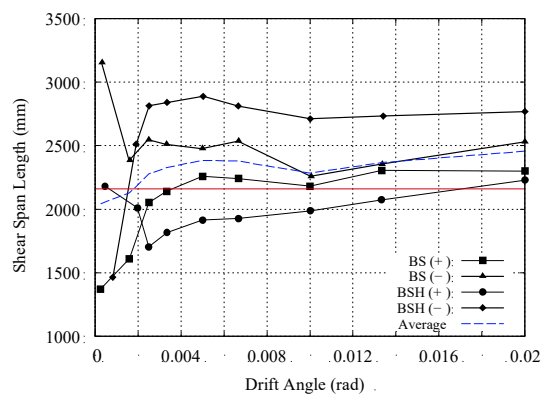


Figure 13. Shear span lengths assumed in the tests for the beam specimen.

3.2.5. Prediction of Shear Strength

As shown previously, the maximum horizontal load can be reasonably well estimated by performing cross-sectional analysis considering force equilibrium. However, since there is no anchored reinforcing in the walls, the strength calculation should be simple to estimate for design, by considering only the tensile stresses of the longitudinal reinforcements and the axial load. To simplify the calculations, it can be assumed that all the longitudinal reinforcements yielded at the maximum load, as shown in Figure 14. The tensile force T by all the longitudinal reinforcements and the axial load P were assumed at the center of the gross member area. The compression force, C , was the sum of the tensile force of the longitudinal reinforcement combined, T , and the member axial load. The neutral axis depth, c , was calculated using Equation (1), which assumes that c is less than the depth of the wall and that the concrete stress block has a depth of $0.85f'_c$. The compression force C acted at the center of the stress block. The bending moment around the center of the member was given by Equation (2). It should be noted that the longitudinal wall reinforcement was not considered in the calculations for tension and compression, and the concrete was neglected in the calculation for tension.

$$c = \frac{C}{0.85f'_c b_w} \quad (1)$$

$$M = C \cdot \left(\frac{D}{2} + D_w - \frac{c}{2} \right) \quad (2)$$

where b_w is thickness of the wall; D is depth of the structural member; D_w is length of the wall.

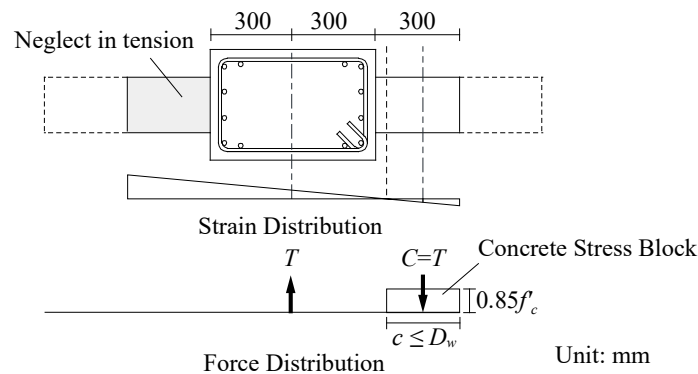


Figure 14. Schematic diagram of the forces on the cross-section.

Table 4 shows the horizontal load-carrying capacity predicted using cross-sectional analysis and Equation (2). As shown in Table 4, the predicted neutral axis depth nearly corresponded to what is shown in Figure 9. The shear force was calculated using the moment and the shear span length, L . The prediction from the cross-sectional analysis underestimated the maximum horizontal load for the BS, but overestimated that for the specimen BSH. The prediction from Equation (2) was either identical or nearly identical to that from the cross-sectional analysis for the beam.

Table 4. Prediction of shear strength.

Property	Specimen	
	BSH	BS
Maximum observed shear strength from the test	285 kN	313 kN
Predicted shear strength by cross-sectional analysis (Bending moment)	301 kN (651 kN·m)	301 kN (651 kN·m)
Tension force T	1367 kN	
Compression force C	1367 kN	
Neutral axis depth c	288 mm	268 mm
Predicted shear strength by Equation (2) (Bending moment)	289 kN (637 kN·m)	295 kN (623 kN·m)

4. Dynamic Evaluation of the Proposed Detailing Method

The detailing method for the fabricated specimens, which were constructed based on the structural member of a real building, was used in the construction of an experimental three-story building. The building was tested by Japan's National Institute for Earth Science and Disaster (NIED) at the E-defense shake-table testing facility. One of the key objectives was to evaluate the performance of the proposed detailing method for hanging walls under dynamic waves in a real building, and another was to validate the new guidelines for important buildings with post-disaster functionality [5]. While there were other objectives in the experiment, such as checking the performances of other non-structural elements (i.e., ceilings) and evaluating structural health monitoring methods, they are outside the scope of this paper and will not be discussed.

4.1. Test Specimen

The specimen was a three-story frame resisting structure with non-structural reinforced concrete wall segments, such as wing and spandrel walls, casted monotonically with structural members (see Figure 15a). The building had two spans in the direction in which shaking was applied and one span in the out-of-plane direction, as shown in Figure 15b. The columns were designated as C1 (central columns) or C2 (outer columns); they all had the same gross cross-sectional dimensions of 600×520 mm, but with different reinforcing layouts. The main beams parallel to the loading direction

were labelled G1 and G1a (reverse of G1) with dimensions of 320 by 480 mm. Beams in the out-of-plane direction were G2 and G3 (280 × 480 mm), while the secondary beam in the in-plane direction was B1 (320 × 400 mm). For walls, the wing walls had dimensions of (180 × 480 mm) and were attached to the columns, and the hanging walls (180 × 400 mm) and standing wall (180 mm × 880 mm) were attached to the beams as shown in Figure 16.

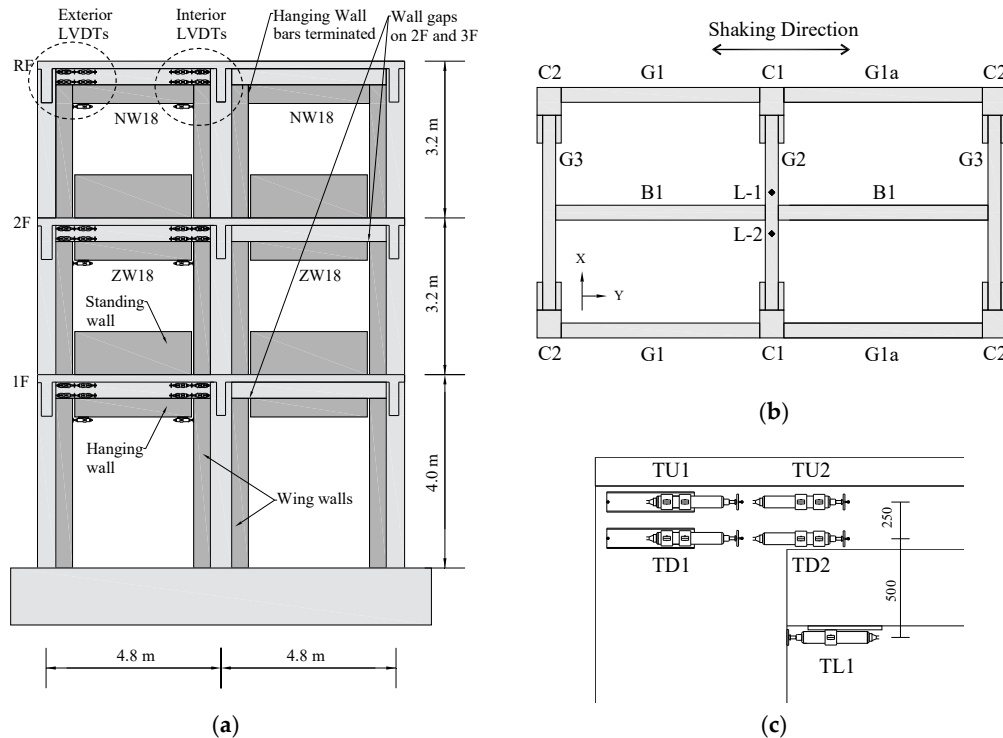


Figure 15. E-defense specimen: (a) in-plane frame; (b) floor plane; (c) exterior LVDTs.

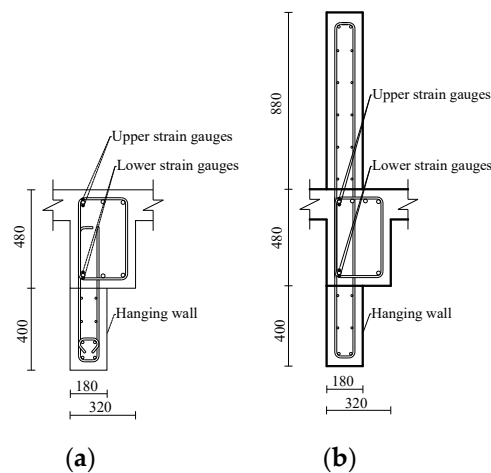


Figure 16. Cross section of the hanging wall: (a) NW18; (b) ZW18, Unit: mm.

To evaluate the performances of the spandrel/hanging walls in both the existing and proposed detailing methods under shaking excitations, the walls were casted to be monolithic, and structural beams with seismic slits were present at the ends of these walls at the wing–wall interfaces on the first and second floors; on the third floor, there was no seismic slit but longitudinal reinforcing bars were not anchored, as shown in Figure 15a. The tie bars were placed at the boundary of the third floor hanging walls, as shown in Figure 16a, to inhibit buckling. Cyclic load reversals may lead to buckling of boundary longitudinal reinforcement, even in cases in which wall boundaries do not

require special boundary elements. Therefore, ties are required for walls with moderate amounts of boundary longitudinal reinforcement, to inhibit buckling [8]. A larger spacing between ties was used owing to lower deformation demands on the walls. The hanging wall reinforcement details are shown Table 5.

Table 5. Hanging walls—reinforcement details.

Name	Third Floor	First and Second Floors
Type of member ($B \times D$)	Beam (320 mm \times 480 mm)	
Long. reinforcement	6-D19 (SD345) $\rho_g = 1.1\%$	
Trans. reinforcement	D10@160(SD295A) $\rho_t = 0.28\%$	
Wall type (Thickness)	Spandrel Walls (180 mm)	
Height of hanging wall	400 mm	
Height of standing walls	-	880 mm
Long. wall reinforcement	4-D13, 4-D10 (1.1%)	2-D13, 4-D10 (0.75%)
Trans. wall reinforcement	D10@160 (0.5%)	D10@160 (0.5%)

The specimen was tested by applying artificial waves five times with different scale factors over three days of testing (two on the first day, one on the second and the final two on the third). White noise excitations were applied at the start and end of each day and between consecutive excitations (eight total) to track changes in the building's dynamic properties resulting from incurred damage during each shaking event. However, as the focus of this study was on the behavior of specific structural elements, results using white-noise excitations will not be discussed. For artificial waves, applying scale factor 1 waves would make its response spectrum equivalent to the design spectrum used in the Japanese building code for ordinary buildings [11]. As shown in Table 6, the first test used a scale factor of 0.2 (20% designed waves) and was performed to confirm that the building could achieve serviceability requirements for frequent shaking events. The second excitation had a scale factor of 1.0 (100% designed waves) to assess whether the building would remain elastic with a peak inter-story drift of less than 0.3%, which is a requirement for buildings with post-disaster functions at code-level shaking. The third test had a scale factor of 1.5 (150% designed waves), which was representative of the design demands for buildings with post-disaster functions. This level of shaking was repeated for the fourth test to evaluate whether the building was capable of withstanding an aftershock at an intensity equal to its design demand, as required by the Japanese building standards. The final excitation had a scale factor of 1.6 (160% designed waves) to observe the building's performance (both structural and non-structural) in its fully inelastic range and its capability to withstand multiple significant seismic events.

Table 6. Expected response of the building.

Number of Trails	Max Designed Acceleration	Scale Factor	Expected Response of the Building
1	5.95 m/s ²	0.2	Serviceability should be maintained for frequent earthquakes
2		1.0	Story drift limit should be less than 0.33%.
3		1.5	Story drift limit should be less than 1.5%
4		1.5	Building should survive an aftershock of equal intensity to the main shock (1.5 times code-level for buildings with post-disaster functionality)
5		1.6	To observe performance of both structural and non-structural elements in its fully inelastic range and its capability to withstanding multiple significant seismic events.

4.2. Test Results

The performance of the building was evaluated through lateral drift level and its member response under the action of dynamic waves carried out on a shaking table. Story drift was measured using laser transducers L-1 and L-2 installed at the geometrical center at the roof and slab of every story, as shown in Figure 15b, and LVDTs installed at locations expected to incur more damage. LVDTs installed at the exterior wall-column showed larger story drift compared to the interior LVDTs, as shown in Figure 15a, but had smaller story drift compared to the laser transducers in second and third floors, as shown in Table 7. This difference might be due to the angular deviation of the beam element during shaking, which could not be recorded directly by the LVDT. However, both drift and angular rotation records were comparable, as shown in Figure 17. Thus, from all these measurements, the maximum and minimum story drifts were found to occur in the first floor and at the top of the building, respectively.

Table 7. Story drift and angular rotation of the hanging walls.

Number of Stories	Story Drift (%)	Beam Rotation by LVDT (%)		Rotation/Story Drift (Exterior LVDT)	Rotation/Story Drift (Interior LVDT)
		Exterior LVDT	Interior LVDT		
1	3.46	3.60	2.53	1.04	0.73
2	3.29	3.13	2.10	0.95	0.64
3	1.70	0.99	0.36	0.59	0.21

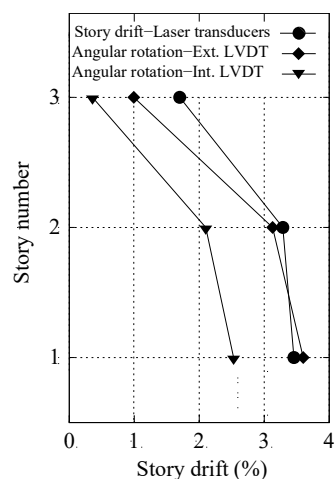


Figure 17. Story drift under the 160% design wave.

Due to the high stiffness of the column/wing-wall components, the rotation angle of a beam member could be considered as being similar to the story drift angle of the same story. Hence, the ratios between the rotation angle of hanging walls and the story drifts indicate the effectiveness levels of the different types of hanging walls, as shown in Table 7. When the ratio is closer to one, the angular rotation is nearly equal to the story drift level in the wall. Conversely, a smaller ratio indicates that the angular rotation of the beam is less than that of the story drift. A lower ratio of story drift to angular rotation of beam, indicates that the hanging wall is capable of restricting inelastic deformation. As can be seen in Table 7, the ratio between hanging wall rotation and story drift was smaller in the third floor where the hanging wall was constructed based on the proposed detailing method.

Members' responses were recorded using strain gauges, which were installed at different locations in each structure member. Performances of the beam members, including hanging walls, were evaluated using average records of the upper and lower strain gauges attached at both sides of the top longitudinal reinforcement, as shown in Figure 16. The average of the first and second floors' story drifts, and the average of the second and third floors' story drifts, were used for the first and second stories' beam members respectively; and the third floor story drift was used for the roof floor beam member.

The relationships between the average drifts and strains of the beams in every story were compared in Figure 18.

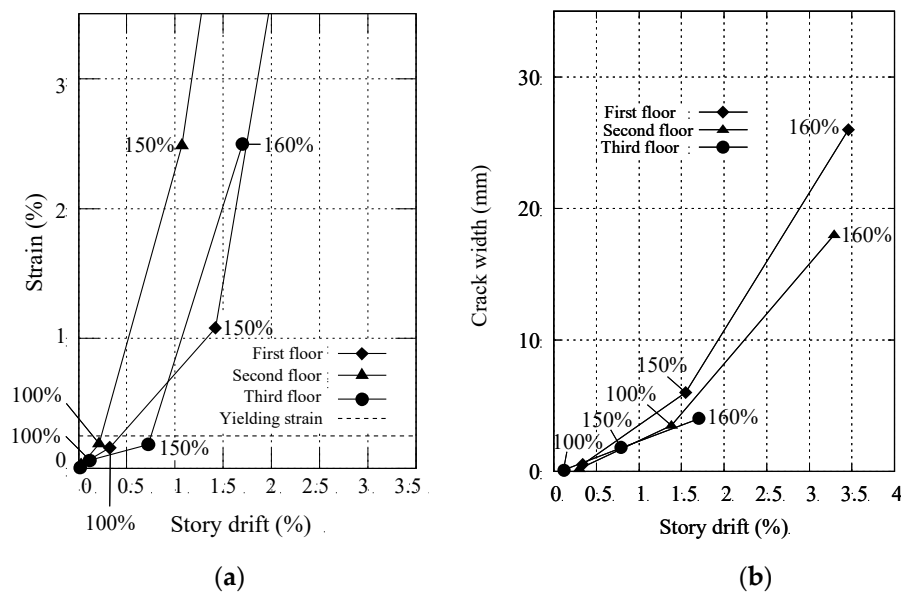


Figure 18. Comparisons of the hanging walls under different earthquake waves: (a) story drift–strain; (b) story drift–crack widths.

As can be seen in Figure 18a, compared to the hanging walls of the first and second floors, the hanging wall of the third floor provided higher strength to the beam, which resulted in a relatively smaller strain at higher drift before the yielding of the longitudinal reinforcement. Likewise, it was observed that the existence of the spandrel walls in the first and second floors could not restrict the formation of the plastic hinges in the critical zone of the beam members. This means that the spandrel walls of the first and second floors were found to be not so effective on the member stiffness of beam components due to presence of the seismic slit. The post yielding performances of the beams shown in Figure 18a were different from those of the pre-yielding state due to unstable strain gauge records for post-yielding state; hence, comparison with the post yielding state might not be practical. The hanging wall with proposed method of detailing was observed at the critical zone under compression load resulted from lateral dynamic waves.

Following the 100%, 150% (first run) and 160% excitations, damage observations and residual crack measurements were performed. Smaller crack widths were observed in the third floor compared with those in the first and second floors at similar story drifts, as shown in Figure 18b. Hence, the damages and strains on hanging walls using the proposed detailing method were found to be satisfactory compared to those on hanging wall with seismic slits.

The beam with a hanging wall showed different damage patterns in the dynamic and static load tests. Previous studies showed that reinforced concrete elements that failed in flexure under static load could fail in shear under dynamic load [12]. Dynamic loads that result in different types of damages to the reinforced concrete element generally refer to waves emerging from blasting and other civil activities. Thus, the beams tested in this study experienced comparable damage patterns (Figures 8 and 19c) and nearly equal cracking widths (Figures 9a,b and 18b) under static and dynamic loads during similar drift periods.

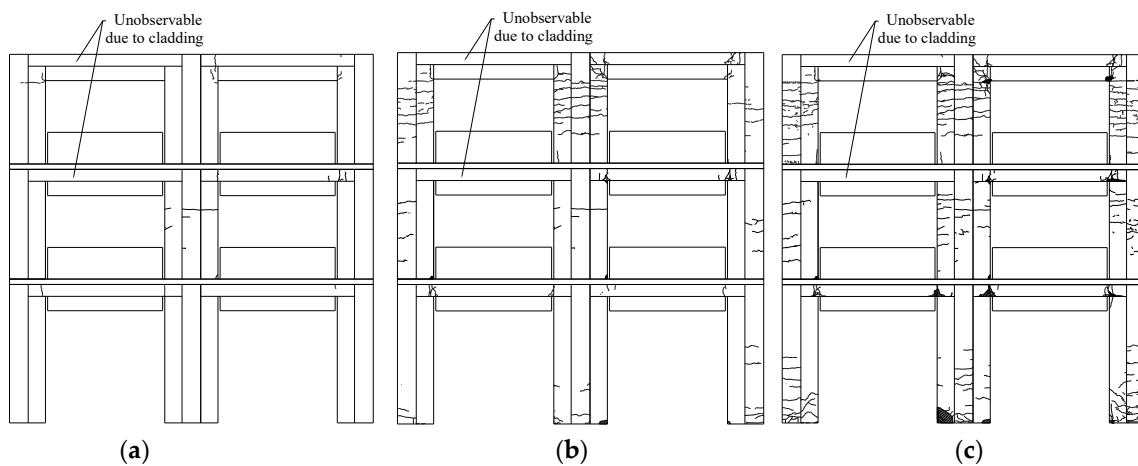


Figure 19. Damage observation of the frame: (a) at 100% of the designed waves; (b) at 150% of the designed waves; (c) at 160% of the designed waves.

The observed cracking patterns for the hanging wall are shown in Figure 19. In the first and second story, diagonal cracks in hanging walls formed and originated at the corner of the slit under 100% shaking intensity. When the first 150% shaking intensity was applied, propagation of big cracks around the slit area, and spalling of the concrete, occurred. When 160% of the designed wave was applied, big hinges occurred in the slit area and spalling of concrete increased. Cracking in the third floor hanging walls appeared in the wall boundary when 100% of the designed waves was applied. Although the cracks did not spread around the wall segments joint area at 150% of the designed waves, the cracks' widths increased. At 160% of the designed waves, minor spalling of concrete occurred and crack widths increased. Thus, the designed waves resulted in formation of dissimilar types of cracks in hanging walls with and without slit as shown in Figure 20. As can be seen, cracking occurred on the column members of top floor, most of which are superficial and do not declare any unusual behavior.

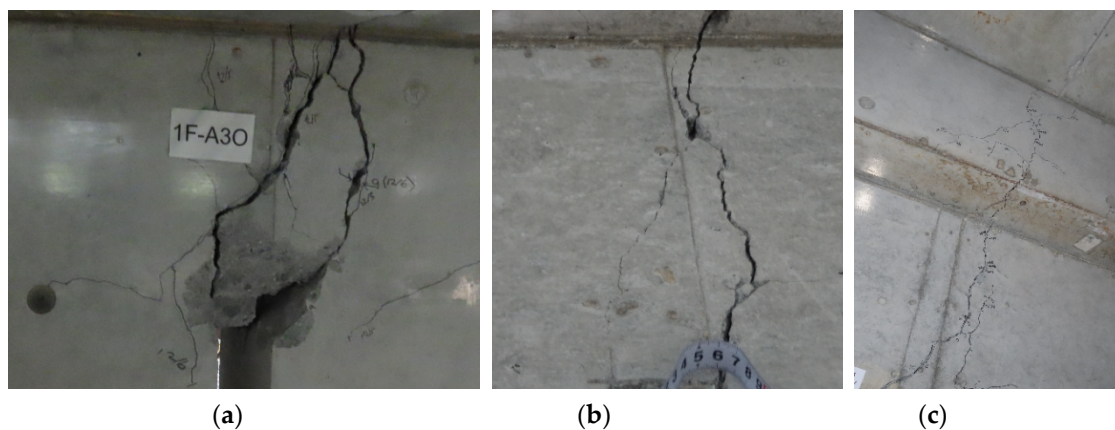


Figure 20. Damage at hanging walls under 150% of the designed waves: (a) first floor; (b) second floor; (c) third floor.

5. Conclusions

Significant seismic events in recent past in Japan have driven the Japanese Building Code to increase the required design base shear and drift limits, especially for buildings to be used in post-disaster management. This requirement is intended to reduce or minimize the vulnerability of non-structural walls during seismic events. A method that increases the potential capability of the non-structural walls and improves the possibility of continuous use of such buildings, is suggested in this study.

The method suggests of connecting monolithically casted non-structural walls with adjacent elements without seismic slits. The method further suggests not to anchor the longitudinal reinforcement to the adjacent columns or wing walls.

The static experiment conducted proved the applicability of the proposed method. It was observed during the experiment that the reduction of seismic slit along with non-anchorage of the longitudinal reinforcement, triggers the non-structural walls to increase the capability of the member instead of being isolated. The method also curtailed the premature damage and vulnerability of the non-structural walls.

The confinement reinforcing impact was not observed on the strength and drift capacity of the beam member, owing to the large number of transverse reinforcements. However, the confinements limited the damage and nearly prevented concrete crushing. The dynamic test results indicated that beam members with non-structural hanging walls based on the existed method were more vulnerable during artificially generated earthquakes compared to other structural members. The responses of hanging walls regarding damage level and strain in a beam under artificially generated earthquakes using the proposed detailing method were found satisfactory compared to hanging walls with seismic slits.

Moreover, the maximum horizontal load of a specimen can be predicted by cross-sectional analysis. The authors propose a simple equation to predict it with sufficient accuracy.

Author Contributions: Investigation, Y.S. and I.N.; methodology, K.K.; project administration, K.K., I.N., T.M. and S.F.; supervision, Y.H.; validation Y.H.; writing—review and editing, W.A.S. All authors have read and agreed to the published version of the manuscript.

Funding: This research received no external funding.

Acknowledgments: This work was partially supported by the Tokyo Metropolitan Resilience Project of National Research Institute for Earth Science and Disaster Resilience (NIED). The authors would like to thank Trevor Zhiqing Yeow for reviewing the paper and his assistance during investigation. Also we thank Y. Mori for providing assistance with conducting the tests at Hiroshima University.

Conflicts of Interest: The authors declare no conflict of interest.

References

1. Architectural Institute of Japan. *Preliminary Reconnaissance Report of the 1995 Hyogoken-Nanbu Earthquake*; English ed.; Architectural Institute of Japan: Tokyo, Japan, 1995.
2. Masaki, M.; Hamood, A.; Kazuki, S.; Kanako, T. Damage of RC Building Structures due to 2011 East Japan Earthquake. In *Proceedings of the Structures Congress 2012*, Chicago, IL, USA, 29–31 March 2012; pp. 1023–1034.
3. Yoon, R.; Sanada, Y.; Akahaori, T. Seismic performance evaluation of RC moment-resisting frames with typical non-structural walls in japan. *J. Adv. Conc. Technol.* **2017**, *15*, 544–557. [CrossRef]
4. Fujii, K.; Yoshida, S.; Nishimura, T.; Furuta, T. Observations of damage to Uto City Hall suffered in the 2016 Kumamoto Earthquake. In *Proceedings of the 8th European Workshop on the Seismic Behavior of Irregular and Complex Structures*, Bucharest, Romania, 17–18 October 2017; pp. 19–20.
5. National Institute for Land and Infrastructure Management (NILIM). *Design Guidelines for Buildings at Disaster Bases (Draft in Japanese)*. Available online: <http://www.nilim.go.jp/lab/bcg/siryou/tnn/tnn1004pdf/ks100414.pdf> (accessed on 4 March 2020).
6. Tsubaki, M.; Sanda, Y.; Zhang, Z.; Kusunoki, K.; Hibino, Y. Experimental structural performance evaluation of RC columns with wing walls without wall vertical rebar anchorage. *J. Struct. Constr. Eng.* **2019**, *84*, 1881–18153. (In Japanese) [CrossRef]
7. Architectural Institute of Japan. *AJ Standard for Lateral Load-Carrying Capacity Calculation of Reinforced Concrete Structures (Draft)*; Architectural Institute of Japan: Tokyo, Japan, 2016.
8. American Concrete Institute. *Building Code Requirements for Structural Concrete (ACI 318-14) and Commentary (ACI 318R-14)*; American Concrete institute: Farmington Hills, MI, USA, 2014.
9. Bentz, E.; Collins, M.P. *Response 2000*; Version 1.0.5; University of Toronto: Toronto, ON, Canada, 2001.
10. Popovics, S. A Numerical Approach to the Complete Stress-Strain Curve of Concrete. *Cement Conc. Res.* **1973**, *3*, 583–599. [CrossRef]

11. The Building Center of Japan (BCJ). *The Building Standard Law of Japan on CD-Rom*; The Building Center of Japan: Tokyo, Japan, 2016.
12. Magnusson, J.; Hallgren, M.; Ansell, A. Air-Blast-loaded High-Strength Concrete Beams, Part I: Experimental Investigation. *Magaz. Conc. Res.* **2010**, *62*, 127–136. [[CrossRef](#)]



© 2020 by the authors. Licensee MDPI, Basel, Switzerland. This article is an open access article distributed under the terms and conditions of the Creative Commons Attribution (CC BY) license (<http://creativecommons.org/licenses/by/4.0/>).